Direct Real-Time Monitoring of Stage Transitions in Graphite Intercalation Compounds

Ayrat M. Dimiev,[†] Gabriel Ceriotti,[†] Natnael Behabtu,[‡] Dante Zakhidov,[†] Matteo Pasquali,[‡,⊥,*] Riichiro Saito,[∥] and James M. Tour[†,§,⊥,*]

Departments of [†]Chemistry, [‡]Chemical & Biomolecular Engineering, [§]Mechanical Engineering and Materials Science, Computer Science, and the [⊥]Smalley Institute for Nanoscale Science and Technology, Rice University, MS-222, 6100 Main Street, Houston, Texas 77005, United States and [∥]Department of Physics, Tohoku University, Sendai 980-8578, Japan

ABSTRACT Graphite intercalation compounds (GIC) possess a broad range of unique properties that are not specific to the parent materials. While the stage transition, changing the number of graphene layers sandwiched between the two layers of intercalant, is fundamentally important and has been theoretically addressed, experimental studies revealed only macroscopic parameters. On the microscale, the phenomenon remains elusive up to the present day. Here we monitor directly in real time the stage transitions using a combination of optical microscopy and Raman spectroscopy. These direct observations yield several mechanistic conclusions. While we obtained strong experimental evidence in support of the Daumas–Herold theory, we find that the conventional interpretation of stage transitions as sliding of the existing intercalant domains does not sufficiently capture the actual phenomena. The entire GIC structure transforms considerably during the stage transition. Among other observations, massive wavefront-like perturbations occur on the graphite surface, which we term the tidal wave effect.

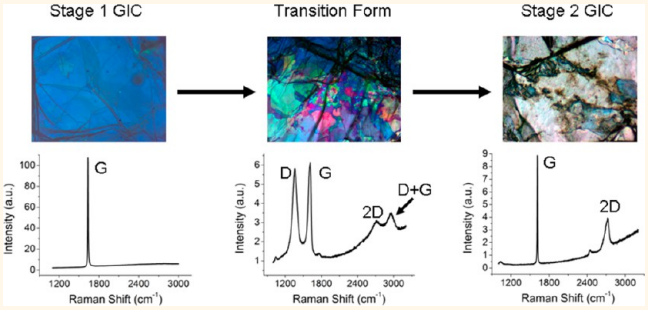

KEYWORDS: graphite intercalation compounds · graphene · stage transition mechanism · Raman spectroscopy · D band origin

Graphite intercalation compounds (GICs) are formed when several atomic, ionic, or molecular species (intercalants) are inserted between the graphene layers of the host graphite. The resulting compounds can be considered as stacks of individual doped graphene layers, easily obtainable in bulk quantities. GICs possess unique properties that are not found in the parent materials.[1,2] The number of graphene layers, *n*, sandwiched between the two layers of intercalant is referred to as the stage number, and the corresponding GICs are called stage *n* GICs. The stage transition, changing the structure of the GIC, has been one of the most intriguing phenomena in GIC-related studies. Theoretically, the stage transition can be understood in terms of the Daumas–Herold (DH) model.[3] According to the DH model, for any GIC with $n > 1$, the intercalant does not occupy the entire graphite gallery but forms islands, called domains. For a stage transition, the intercalant does not need to be completely removed from one gallery and reinserted into another gallery. Instead, the islands of intercalant simply slide along the graphite galleries to convert one stage into another. Despite numerous theoretical studies performed to address the stage transition,[4−6] the proposed models do not fit well with the experimental data. Yet, experimental studies have revealed only macroscopic parameters,[7−9] and the dynamics of intercalation remains elusive on the microscale. Here we study the microscale dynamics in real time by monitoring the stage transitions with optical microscopy and Raman spectroscopy.

The sulfuric acid GIC (H_2SO_4-GIC) remains one of the least studied and poorly understood GICs. Unlike many other substances, H_2SO_4 does not spontaneously intercalate into graphite, as the reaction has a positive Gibbs free energy.[10] The H_2SO_4-GIC can be produced only by means of anodic or chemical oxidation.[7−15] Here we prepared stage 1

* Address correspondence to mp@rice.edu, tour@rice.edu.

Received for review January 14, 2013 and accepted February 26, 2013.

Published online February 26, 2013
10.1021/nn400207e

GIC by exposing graphite to a solution of ammonium persulfate in sulfuric acid $(NH_4)_2S_2O_8-H_2SO_4$. As we showed earlier,[16] with the use of this chemical mixture, the GIC formation is highly reversible and does not lead to formation of a graphite oxide byproduct. Thus, this system can serve as a testbed for the real-time monitoring of graphitic structural changes.

In our experimental work, we studied both processes: direct intercalation and reverse deintercalation. We focused mostly on stage 2 to stage 1 transitions because the two stages and their mixtures have distinct colors, making the transition easily observable using an optical microscope. In our previous report, we carefully characterized the blue stage 1 GIC and the white stage 2 GIC by Raman spectroscopy and X-ray diffraction (XRD).[16] Here we focus on the transition from one stage to the other. To initiate intercalation, a graphite flake was immersed into the $(NH_4)_2S_2O_8-H_2SO_4$ solution. To initiate deintercalation, the $(NH_4)_2S_2O_8-H_2SO_4$ solution surrounding the flake was diluted with water. Optical images obtained during intercalation were of lower quality when compared to those during deintercalation because intercalation was slower and gas bubbles generated by the $(NH_4)_2S_2O_8-H_2SO_4$ mixture obscured the graphite surface. Thus, the higher quality deintercalation images are shown here, and the intercalation images are available in the Supporting Information. We find that the sequence of phenomena occurring during deintercalation generally is the opposite of that which occurs during intercalation.

RESULTS AND DISCUSSION

To monitor the stage 1 to stage 2 transition, a thin intercalated graphite flake suspended in the $(NH_4)_2S_2O_8-H_2SO_4$ solution was sandwiched between the two microscope slides, as shown in Figure 1a.

Deintercalation of the stage 1 GIC was induced by controlled dilution of the $(NH_4)_2S_2O_8-H_2SO_4$ solution with water. Figure 1 and video S1 (Supporting Information) show the typical stage 1 to stage 2 transition recorded at low magnification, where one can see the staging transformation over an entire graphite flake. The stage transition begins on the right edge of the flake and propagates toward the opposite edge. The transformation is accompanied by two distinct and independent phenomena: (a) structural deformations and (b) color change. The stage transition is directional (right to left) because the $(NH_4)_2S_2O_8-H_2SO_4$ solution was diluted from the right side, thus inducing a directional concentration gradient. In the case of direct intercalation (Figure S1), the solution concentration is the same all around the flake, and the stage transition begins simultaneously around the entire flake perimeter. Note that in both cases (Figure 1 and Figure S1) the stage transition begins from the edge and not from an area in the middle of the flake despite the fact that the entire flake is immersed in the solution.

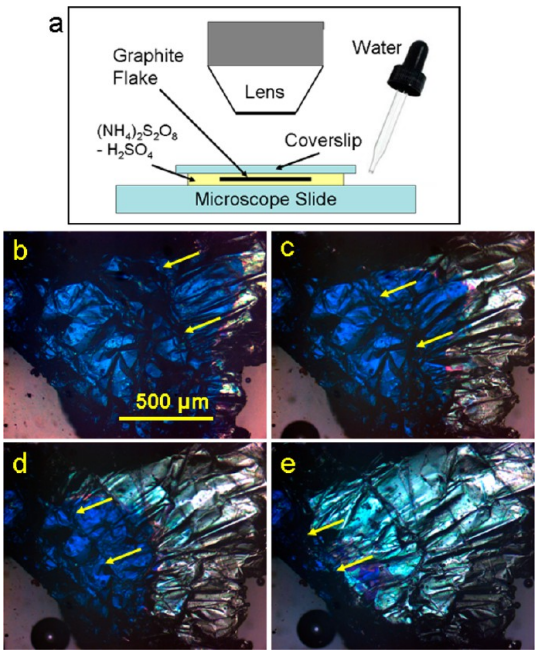

Figure 1. Stage transition recorded at low magnification. (a) Schematic of the optical cell used to monitor the stage transitions. Controlled dilution of the $(NH_4)_2S_2O_8-H_2SO_4$ solution from one selected side induces the concentration gradient. (b–d) Micrographs taken at 40 s time intervals show the stage transition recorded at low magnification. The transition front propagates from right to left. The yellow arrows point at the leading edge of the transition front, which manifests as a mechanical deformation.

These observations contradict earlier suggestions[7] that intercalant crosses the C-face through grain boundaries and defects.

Figure S2 and Figure 2 are from intercalation and deintercalation events, respectively, recorded at higher magnification than Figure S1 and Figure 1, revealing additional details of the phenomenon (see Supporting Information video S2 for the entire deintercalation process). The stage 2 to stage 1 transition (Figure S2) is the opposite of the transition from stage 1 to stage 2, discussed below (Figure 2). The stage 1 to stage 2 transition begins (Figure 2) with mechanical deformation of the flake surface, which appears as a wave moving across the surface of the sample; this large wave-like movement is referred to here as the "tidal wave effect". As the tidal wave propagates through the imaged area, it leaves folds that resemble wrinkles. These folds are aligned in the direction of wave propagation, perpendicular to the wave, and largely dissipate by the end of the transformation (Figure 2f). Thus, the stage transition causes severe mechanical deformation of the graphite surface. The original surface in front of the wave is flat; the tidal wave area itself is heavily crumpled, and the area behind it is stretched and folded. Careful examination of the tidal wave (Figure 2a–d and Figure S2) reveals that the top deforming layer is transparent, and no color change occurs inside this layer. This suggests that it is likely composed of only one graphene layer.

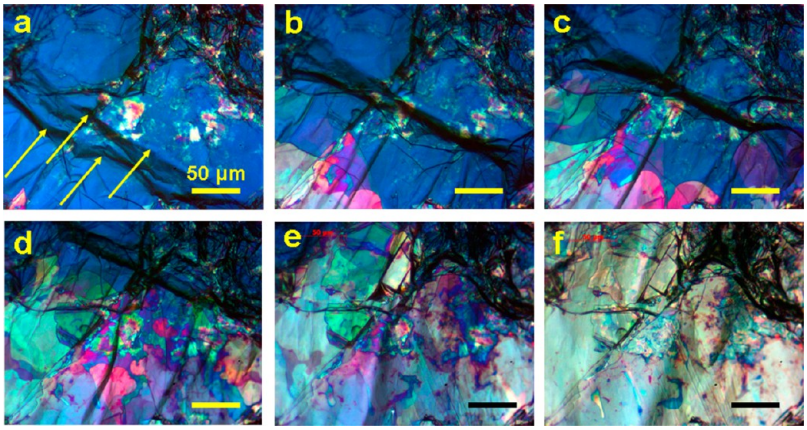

Figure 2. Stage transition recorded at higher magnification. (a) Photograph showing the beginning of the stage transition. The transformation front propagates from the bottom left to the top right corner in the direction indicated by the yellow arrows. The photos in panels (b) 26 s, (c) 33 s, (d) 56 s, (e) 90 s, and (f) 120 s were taken from the same area as (a) at the indicated time intervals after photograph (a). The yellow arrows on panel (a) point to the two dark wavy stripes where the graphite surface is deformed and crumpled. The bright colors in panels (b–d) are the areas of the mixed stage 1 and 2. The color depends on the number of the intercalant layers that have been removed. The neutral colors in panels (e,f) indicate a stage 2 condition. The entire flake was ~1 mm in size.

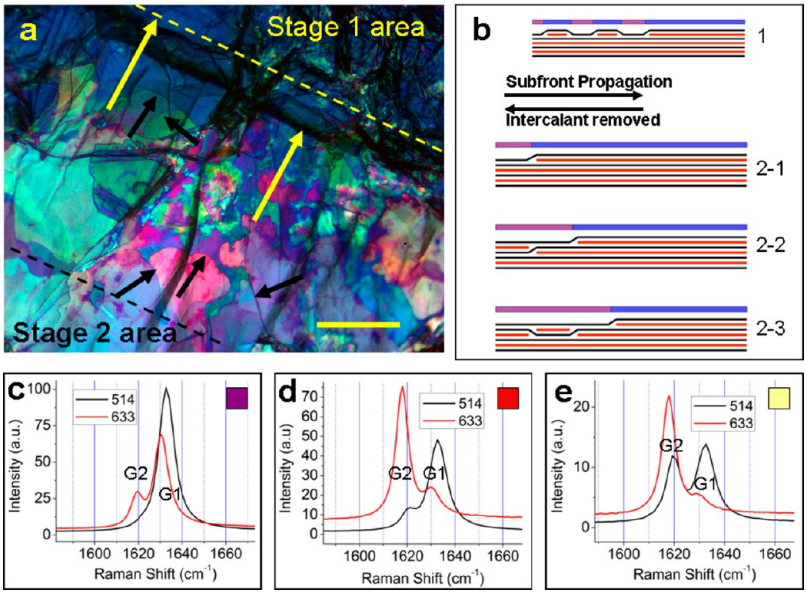

Figure 3. Study of the transition zone. (a) Photograph showing the transition zone. The yellow and black dashed lines represent the leading edge and the tailing edge of the transition zone, respectively. The two yellow arrows point at the top and the bottom of the tidal wave and show the general direction of the front propagation. The black arrows show the direction of the subfront propagation and point at the edge of the subfronts. The scale bar is 50 μm. (b) Schematics of the stage transition for the subfront propagation. The black lines are the carbon layers; the red lines are the layers of intercalant. The schematic 1 on top shows the unlikely scenario of the stage transition with a single deintercalating gallery. The schematics 2-1 to 2-3 show three consecutive steps of the stage transition occurring with respect to the DH theory. The colored stripes above the models are the colors of the graphite surface as seen in the optical micrograph. (c–e) Raman spectra taken from the violet, red, and ivory spots, respectively, with two different lasers: 514 nm (black line) and 633 nm (red line).

Within the tidal wave boundaries, the top deforming layer progressively delaminated from the rest of the flake. The delaminated area of the top layer loses its transparency and appears dark. Transparency is fully recovered when the top layer re-adheres to the main body of the flake. This observation demonstrates the possibility for layer-by-layer exfoliation of graphite *via* repetition of the intercalation–deintercalation process.

Following ~50 to 100 μm behind the tidal wave, a front of bright rainbow colors propagates through the area. We refer to this broad colorful band separating the original blue stage 1 area from the white stage 2 area as the "transition zone" (Figure 3a). The leading edge of the transition zone is the tidal wave; it is well-defined. The trailing edge is the imaginary border between the rainbow-colored areas and white area; it is indicated by a black dashed line in Figure 3a. Each single

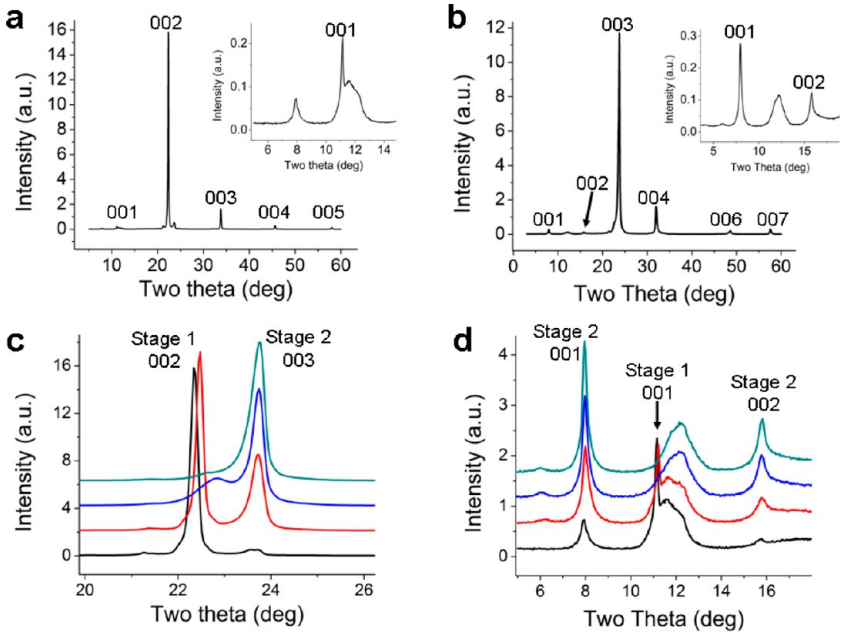

Figure 4. X-ray diffraction patterns of stage 1 and stage 2 GICs. (a) Stage 1 GIC. (b) Stage 2 GIC. The insets show the *Y*-axis expansions in the 5−16° 2θ angle region. (c,d) Transition of stage 1 GIC into stage 2 GIC shown from bottom (black line) to top (navy line). (c) The 20−26° expansion and (d) 5−18° expansion of the same diffraction patterns. The time interval between each of the four acquisitions is ∼24 h. The original stage 1 GIC contains traces of the stage 2 phase due to partial decomposition during the sample transfer and acquisition procedures. All of the XRD data were acquired from the samples sealed under a poly(ethylene terephthalate) film to protect the GIC from immediate decomposition.

brightly colored area propagating within the transition zone is defined as a subfront. Figure 3b depicts the subfront propagation schematically and is discussed below. The Raman spectra taken from the colored areas reveal the mixed stage 1/stage 2 structure (Figure 3c−e). Since the subfront color is uniform within the acquisition spot, the sample has a mixed stage in the *C*-axis direction. The new color appears when the intercalant is removed from a certain number of graphite galleries.

While the general direction of the front propagation remains the same (bottom left to top right), different subfronts propagate obliquely to the tidal wave direction. Often, two subfronts cross each other with no interference. The shape of the subfronts and the rate of their propagation are not the same as the preceding subfronts. These observations indicate that different subfronts represent removal of intercalant from different graphite galleries, and these events occur independently of each other. The colored subfronts always have sharp boundaries, often with dark borderlines separating the two differently colored areas. When the dark borderline is wide enough, one can see that it is actually the steep face of a minor mechanical wave. By overlapping, different subfronts create the observed colorful mosaic. Despite the appearance of a broad variety of colors, there are a limited number of tints that correspond to deintercalation of a certain number of layers. The stage 1 GIC has a 200 nm wide transmission window centered at ∼700 nm.[16] It appears blue in reflected light because it does not reflect the red light. For the stage 2 GIC, the transmission window shifts to the IR region, thus it reflects all visible light and appears white. Hence, at the beginning of the stage transition, a small fraction of emerging stage 2 phase adds the red tint to the original blue color. When the stage 2 content increases, the observed color changes in the sequence: blue, violet, purple, red, light orange, ivory, and white.

Figure 3c−e shows Raman spectra from the three different areas with typical colors. As is evident from Figure 3c−e, both the absolute G1 peak intensity and the G1/G2 ratio decrease when the color progressively changes from blue to white (here and below the G1 at 1633 cm^{-1} and G2 at 1619 cm^{-1} represent the G band of stage 1 and stage 2 phases, respectively). However, we showed in our previous report that the G1/G2 ratio can be used only as a relative representation of stage 1 *versus* stage 2 content.[16] The two peaks are not equally enhanced by the different lasers (see Supporting Information section S2, Figure S3, which is a summary of the earlier reported Raman data[16] for pure stage 1 and stage 2 GICs). The same selective enhancement is observed for the mixed stage conditions (Figure 3c−e). The Raman spectrum taken from the violet spot (Figure 3c) with the 514 nm laser appears the same as for the pure stage 1 compound; no G2 peak was detected. At the same time, the spectrum acquired from the same spot with the 633 nm laser contains a G2 component, suggesting the presence of the stage 2 phase.

While Raman spectroscopy was the main analytical method used to monitor the staging, the stage transition for bulk samples was independently confirmed by XRD analysis (Figure 4). The 22.2° 2θ angle diffraction

line (Figure 4a) is the 002 signal of the stage 1 GIC, which is in good agreement with the 001 signal at 11.2°. The diffraction lines at 33.6 and 45.3° 2θ angles are the 003 and 004 signals, respectively. The calculated *C*-axis repeat distance I_c is 0.801 nm, which is in good agreement with the previously published data.[8,9,12] The thickness of a layer of intercalant is 0.801 nm − 0.335 nm = 0.466 nm. For the stage 2 GIC (Figure 4b), the weak diffraction lines at 8.0 and 16.0° 2θ angle correspond to the 001 and 002 signals, respectively, with a repeat distance of 1.105 nm. The strong diffraction lines at the 24.2 and 32.3° 2θ angles correspond to the 003 and 004 signals, respectively. The 006 and 007 signals are also well observable. Figure 4c,d represents the results of *in situ* measurements taken during the stage 1 to stage 2 transitions. It is evident that, with progression of the stage transition, the intensity of the diffraction lines associated with the stage 1 decreases, while the intensity of the stage 2 signals increases. Thus, the stage 2 phase content increases at the expense of the stage 1 phase, confirming transition of the latter into the former.

The probing depth in Raman spectroscopy for stage 1 H_2SO_4-GIC is ~100 nm.[7] On the basis of this depth, we should detect the signal from ~125 carbon layers. The crystallite thickness values (L_c) calculated from the XRD data (Figure 4) by the Scherrer equation were 32.2 nm for stage 2 GIC and 44.9 nm for stage 1 GIC. The two data points are consistent and suggest the presence of 56 to 57 graphene layers in one crystallite. Removal of one layer of intercalant from such a crystallite results in a GIC with a ratio of stage 1 to stage 2 phases of 54:2 (27:1). This ratio is consistent with the G1/G2 ratio observed in the Raman spectra acquired from violet areas (Figure 3c). Thus, the violet color likely indicates the removal of intercalant from a single graphite gallery. The removal of additional layers of intercalant increases the red tint of the observed color, and the G2/G1 ratio increases (Figure 3d). With deeper deintercalation, the color becomes more neutral and the sample transparency decreases. This results in a decrease of the probing depth and the Raman signal intensity (Figure 3e).

The analysis of subfront propagation suggests new mechanistic conclusions regarding intercalant movement during the stage transitions. While the stage 3 to stage 2 transition is well-explained by domain-type structure in the DH model, the stage 1 to stage 2 transition does not require the existence of domains. It can be accomplished by removing intercalant from every other gallery; no reinsertion into a new gallery is required. In our experiments, the observed subfronts are uniform in tint and intensity. When the subfront passes an area, it replaces the existing color with the new one, suggesting that in a given area the intercalant is being efficiently removed from a certain number of graphite galleries. Figure 3b shows schematics for propagation of a violet-colored subfront over a blue-colored area, signifying removal of only one layer of intercalant from between two graphene layers. Schematic 1 (Figure 3b) shows the scenario with one single deintercalating gallery. If this scenario were realistic, the intercalant moving toward the edge of the flake would have to make openings and squeeze through the previously deintercalated closed gallery. The moving islands of the intercalant should temporarily convert the deintercalated stage 2 area into a stage 1 area and should have been detected in the optical microscope as a fluctuation of color; yet, we never observed these signatures. The mechanism of the stage transition becomes understandable if two (not one) galleries deintercalate simultaneously to remove formally just one layer of intercalant (schematics 2-1 to 2-3 in Figure 3b), as suggested by the DH model. In this case, the intercalant islands (DH domains) slide along the two galleries, separated by a graphene layer. This is supported by the constant stream toward the edge of the flake in a direction opposite the propagation of the transformation front (see Supporting Information videos S1 and S2). Thus, our observations demonstrate that the stage transition occurs in accord with the DH theory, and the resulting stage 2 GIC should have domain-like structure.

The structural transformations associated with stage transitions were further analyzed by Raman spectroscopy. Monitoring the stage transition by Raman spectroscopy is difficult because acquisition of Raman spectra is slow compared to the rate of the transformation. The area within the spectral acquisition spot can be different at the beginning and at the end of the acquisition. To obtain statistically relevant data, we acquired hundreds of Raman spectra while carefully observing the Raman acquisition spot areas before and after acquiring the Raman spectra. Figure 5 shows typical spectra from a stage transition monitored by Raman spectroscopy. One can single out two steps of the stage transition that are shown in Figure 5a,b and in Figure 5c,d, respectively. The first step begins with the appearance of a broad D band, which gradually increases while the stage transition progresses through the acquisition spot (Figure 5a,b). Simultaneously, the G1 band decreases in intensity and a broad shoulder appears toward the lower wavenumbers. Overall, the Raman spectrum changes from that of a stage 1 GIC (black line) to the spectrum shown by the red line (Figure 5a,b). This Raman spectrum contains large and broad D and G peaks and the hump-like features of the two low and broad 2D and D+G peaks. The spectrum is very similar to those of graphite oxide or amorphous carbon with a crystallite size of a few nanometers; hence, we call it a pseudoamorphous state. Conversion of stage 1 GIC into the pseudoamorphous state signifies the first step of the stage transition. During the second step (Figure 5c,d), the D peak gradually decreases and almost disappears. The humps change as the D+G peak decreases, and the 2D peak increases and becomes the size that is normal for stage 2 GIC. The

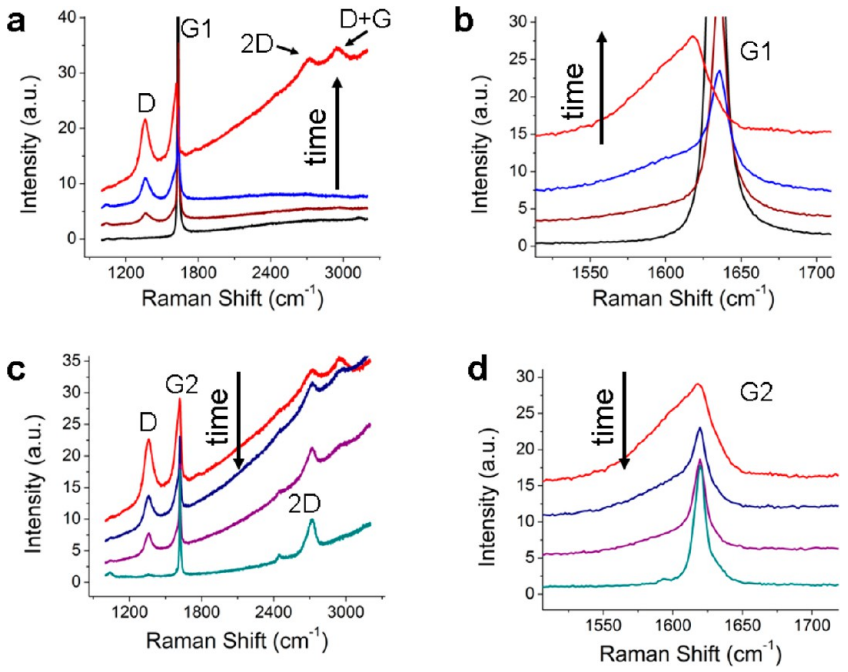

Figure 5. Monitoring stage transition by Raman spectroscopy. (a,b) Transformation from stage 1 GIC (black line) to a transitional pseudoamorphous state (red line). Both (a) and (b) have a truncated *Y*-axis. The top of the G peak for the stage 1 GIC spectrum is at ~100 au on the *Y*-axis scale. (c,d) Transformation from the pseudoamorphous state (red) to stage 2 GIC (dark cyan). The line colors are not related to actual spot colors; they are used to differentiate spectra from each other. Panels (b) and (d) show the G band area of the spectra shown on panels (a) and (c), respectively.

G peak becomes narrow and stays at 1619 cm^{-1}, signifying formation of the stage 2 GIC.

The appearance of the D peak during the stage transition is not trivial and to the best of our knowledge has not yet been reported. The appearance of the D peak signifies the short-range elastic scattering of photoexcited carrier in the real space by the defect structure. The origin of the D band is explained by the double resonance theory in which one of two scattering processes is an elastic, intervalley scattering corresponding to the short-range scattering.[17,18] In our experiments, no permanent structural defects were produced during the stage transition; the process is highly reversible,[16] and carbon remains sp^2-hybridized. The only structural features that can be considered defects are the bending edges of the graphene layers at the DH domain boundaries, also known as domain walls. The I_D/I_G ratio in the spectrum of the pseudoamorphous state is 1.38. The systematic studies made on single-layer graphene with defects induced by Ar^+ bombardment[19,20] showed that this value of the I_D/I_G ratio is reached when the average distance between the two defects is less than 2 nm. Conversely, the D band is difficult to observe when the interdefect distance is larger than 24 nm.[20] Ferrari and Robertson developed eq 1 relating the I_D/I_G ratio to the crystallite size (L_a) of amorphous carbons:[21]

$$I_D/I_G = C'(\lambda)L_a^2 \quad (1)$$

where C' is ~0.0055 for the 514 nm excitation laser and λ is the laser wavelength. The crystallite size calculated with eq 1 is only 0.70 nm. This is comparable to the thickness of a layer of intercalant of 0.466 nm (derived as the difference in interlayer distances between a stage 1 GIC and parent graphite). Note that the D band is not observed in the Raman spectrum of the pure stage 2 GIC (Figures 5c and S3h) or in the spectra of mixed stages when the system is static and resting at equilibrium. The D band arises only when the system is removed from the equilibrium state and intercalant movement begins. We found that the D band intensity (the I_D/I_G ratio) is proportional to the rate of the stage transition, which in turn depends on the degree of dilution. Figure S4 shows that the D band is also present during the stage 2 to stage 3 and the stage 3 to stage 4 transitions that follow the original stage 1 to stage 2 transition. Thus, on the basis of the existing knowledge of Raman spectroscopy, we can conclude that during the stage transitions the size of the DH domains decreases compared to the static state to the size of just a few H_2SO_4 molecules.

At the beginning of the stage transition (spectra shown with brown and blue lines in Figure 5a,b), the decreasing G1 band is still at 1635 cm^{-1} and the 2D band is missing, signifying that the GIC is still at the stage 1 condition. However, some structural changes have already begun, causing the D band to appear. During the second part of the stage transition (navy and purple lines in Figure 5c,d), the system has all of the characteristics of the stage 2 GIC: the emerging G2 band is at 1619 cm^{-1}, and the 2D band is present. The Raman spectrum of the transitional pseudoamorphous

state is very different from those of the stage 1 and stage 2 GICs and cannot be derived by superimposing the two. Correspondingly, the pseudoamorphous state is not a simple mixture of the two phases but an independent structure. In summary, the conventional interpretation of stage transitions as sliding of existing intercalant domains is a simplified version of a more complex phenomenon. Significant transformation of the GIC structure occurs during the stage transition. Note that we arrive at this conclusion based on existing knowledge of the Raman spectroscopy of graphitic materials. Alternatively, the observed data might suggest an unconventional view of the physics of the D band origin.

When H_2SO_4-GIC is prepared by anodic oxidation,[7−12] the intercalation process is controlled by the amount of electricity passed through the circuit. In the chemically induced intercalation described here, the process is quasi-spontaneous. This gives us an additional advantage in exploring stage transitions *via* kinetics studies. The ability to directly monitor the front propagation by optical microscopy affords an accurate measure of the rate of stage transition with much higher accuracy than in the previous kinetics studies.[7−9] We found that the rate of the stage transition can be largely controlled by the electrochemical potential of the solution in which the flake is immersed. Thus, for direct intercalation, an increase of the $(NH_4)_2S_2O_8$ concentration in H_2SO_4 by a factor of 3 increased the rate of stage transition by a factor of ∼9. The chemistry of the $(NH_4)_2S_2O_8$−H_2SO_4 system is not completely clear, but if one assumes that the electrochemical potential is proportional to the second power of the $(NH_4)_2S_2O_8$ concentration, then the observed rate of the stage transition is directly proportional to the electrochemical potential. Using potassium chlorate ($KClO_3$) as an oxidizing agent instead of $(NH_4)_2S_2O_8$ at the same molar concentration increased the rate of intercalation by a factor of 18. For the deintercalation, the rate depended on the degree of dilution of the $(NH_4)_2S_2O_8$−H_2SO_4 solution, or on the solution electrochemical potential. The highest measured instantaneous front propagation rate during the stage 1 to stage 2 transition was 103 μm/s, and typical rates were 2 to 15 μm/s. The rate was highest when the stage transition began at the edge of the flake, and the transition front slowed down as it progressed through the flake. The subfronts and front sometimes recede and then return and proceed in the original direction. This might be induced by instability in the solution concentration gradient caused by chaotic microflow near the flake surface. These observations suggest that the driving force behind the stage transition is electrochemical. The intercalant enters the interlayer galleries when the electrochemical potential favors intercalation, and it is quickly removed when the electrochemical potential becomes lower than a threshold value. At the same time, the behavior of subfronts within the transition zone is not as consistent as the propagation of the front. While the transition front monotonously propagates through the observed area, the subfronts within the transition zone can slow down for several seconds and then skip suddenly ahead or sideways. This subfront behavior can be indicative of the role of the lattice strain in stage transitions. The shapeless concentric form of the subfronts and absence of any directional priorities in their propagation suggest that the process is not dominated by graphite crystalline structure; the intercalant species move in the graphite galleries as between two featureless plates.

CONCLUSION

In summary, we report real-time monitoring of stage transitions in GICs by Raman spectroscopy and optical imaging. Massive tidal wave structural deformations of the graphite surface accompany the stage transitions. The intercalant enters and exits the graphite flake through the edges; earlier suggestions that the intercalant crosses the C-face through grain boundaries and defects are not supported by our data. The stage transition propagates as a front, converting one stage into another. There is a narrow transition zone (50−200 μm) separating two different phases. Within the transition zone, intercalant enters and exits different graphite galleries independently of each other in the form of shapeless concentric subfronts. While we find strong experimental evidence in support of the DH theory, the conventional interpretation of stage transitions as simple sliding of the existing intercalant domains does not reflect the entire complexity of the actual phenomena. Significant changes occur in the intercalant and the GIC during the stage transition. The driving force behind the stage transition is the electrochemical potential of the surrounding media. The intercalant species move in the graphite galleries as between two featureless plates.

METHODS

To prepare the GIC, $(NH_4)_2S_2O_8$ (1.0 g, Sigma-Aldrich) was added to 98% H_2SO_4 (10.0 mL, Fisher Scientific) with constant swirling. The mixing was accompanied by gas evolution from the partial decomposition of the persulfate anion. After 5 min of swirling, flake graphite (0.2 g, Sigma-Aldrich, batch #13802EH) was added to the solution and swirling was continued. Formation of the GIC was signified by the appearance of the deep blue color of the graphite. Complete intercalation was achieved in 4−10 h. To observe deintercalation, a sample of stage 1 GIC with $(NH_4)_2S_2O_8$−H_2SO_4 solution was placed between a microscope slide and the coverslip. Next, the coverslip was slipped back and forth several times under light hand-applied shearing stress to cleave the original intercalated flake to several thinner and smaller flakes. The thickness of the cleaved flakes depends on the pressure applied to the coverslip and on the time of the shearing motion. The intercalated flakes are easily cleaved, thus only slight pressure (a touch with the tip of tweezers) was

applied. The thickness of the flakes cleaved with the light pressure is approximately 10−50 μm. Most of the photographs taken in the reflected light mode were taken of such flakes, and a precise flake thickness was not needed to observe the phenomena discussed here. For transmission light images, however, thinner flakes in the submicrometer thickness range were required, so higher pressure and longer shearing motion were applied to the coverslip to obtain thinner flakes that are semitransparent. As long as sufficient transmitted light could be acquired, the flake was of appropriate thickness for the effects disclosed here. A layer of $(NH_4)_2S_2O_8$−H_2SO_4 solution was always present between the graphite surface and the microscope slide; the graphite flake was free floating in the acid mixture. This was supported by the observation that micrometer-sized air bubbles were floating between the coverslip and the observed graphite surface. Deintercalation was triggered by addition of a drop of water to the edge of the two microscope slides. By this procedure, the diffusion of water into the $(NH_4)_2S_2O_8$−H_2SO_4 solution was limited, and a controlled, slow dilution was accomplished. The dilution was roughly 1 part water per 3−5 parts (v/v) of the original $(NH_4)_2S_2O_8$−H_2SO_4 solution. The transformation normally began in 10 s to 5 min after dilution, depending on the macroscopic geometrical parameters and the degree of dilution. In alternative experiments, deintercalation was observed by exposing the GIC sample to air.

Light micrographs were acquired using the Zeiss Axioplan 2, equipped with AxioCam MRc. The reflection mode was used with a white incandescent light source. Two types of lenses were used: Zeiss Epiplan 10×, 0.2 for low-magnification imaging, and Zeiss LD Epiplan 20×, 0.4 HD DIC for higher magnification. Typically, images were acquired at full light intensity with exposure times ranging between 50 and 400 μs. The Raman spectra were acquired using the Renishaw Raman RE01 microscope with 40× lens. The 514 and 633 nm wavelength lasers were used for excitation. XRD was acquired using a Rigaku D/Max 2550 diffractometer with Cu Kα radiation (λ = 0.15418 nm). The data obtained were analyzed and processed using the Jade 9 software package.

Conflict of Interest: The authors declare no competing financial interest.

Acknowledgment. The work was supported by the AFOSR (FA9550-09-1-0581, FA9550-09-1-0544, and FA9550-09-1-0590), AFOSR MURI (FA9550-12-1-0035), ONR MURI (#00006766, N00014-09-1-1066), the Welch Foundation (C-1668), and the MEXT grant (No. 20241023).

Supporting Information Available: Additional photos, Raman spectra, and digital movies. This material is available free of charge *via* the Internet at http://pubs.acs.org.

REFERENCES AND NOTES

1. Dresselhaus, M. S.; Dresselhaus, G. Intercalation Compounds of Graphite. *Adv. Phys.* **2002**, *51*, 1–186.
2. Enoki, T.; Endo, M. *Graphite Intercalation Compounds and Applications*; Oxford University Press: New York, 2003.
3. Daumas, N.; Herold, A. Notes des Membres et Correspontants et Notes Présentées ou Transmises par Leurs Soins. *C. R. Acad. Sci. Ser. C* **1969**, *268*, 373–375.
4. Moret, R. In *Intercalation in Layered Materials*; Dresselhaus, M. S., Ed.; NATO ASI Series, Ser. B: Physics; Plenum: New York, 1986; Vol. 148.
5. Millman, E.; Kirczenow, G. Origin of Simple Staging in Graphite Intercalation Compounds. *Phys. Rev. B* **1982**, *26*, 2310–2313.
6. Safran, S. A. Cooperative Effects and Staging in Graphite Intercalation Compounds. *Synth. Met.* **1980**, *2*, 1–15.
7. Eklund, P. C.; Olk, C. H.; Holler, F. G.; Spolar, J. G.; Arakawa, E. T. Raman Scattering Study of the Staging Kinetics in the C-Face Skin of Pyrolytic Graphite-H_2SO_4. *J. Mater. Res.* **1986**, *1*, 361–367.
8. Yosida, Y.; Tanuma, S. *In Situ* Observation of X-ray Diffraction in a Synthesis of H_2SO_4-GICs. *Synth. Met.* **1989**, *34*, 341–346.
9. Nishitani, R.; Sasaki, Y.; Nishina, Y. Kinetics of Staging Transition in H_2SO_4-Graphite Intercalation Compounds. *Synth. Met.* **1989**, *34*, 315–321.
10. Aronson, S.; Frishberg, C.; Frankl, G. Thermodynamic Properties of the Graphite-Bisulfate Lamellar Compounds. *Carbon* **1971**, *9*, 715–723.
11. Metrot, A.; Fischer, J. E. Charge Transfer Reactions during Anodic Oxidation of Graphite in H_2SO_4. *Synth. Met.* **1981**, *3*, 201–207.
12. Besenhard, J. O.; Wudy, E.; Möhwald, H.; Nickl, J.; Biberacher, W.; Foag, W. Anodic Oxidation of Graphite in H_2SO_4. Dilatometry−*In Situ* X-ray Diffraction−Impedance Spectroscopy. *Synth. Met.* **1983**, *7*, 185–192.
13. Inagaki, M.; Iwashita, N.; Kouno, E. Potential Change with Intercalation of Sulfuric Acid into Graphite by Chemical Oxidation. *Carbon* **1990**, *28*, 49–55.
14. Moissette, A.; Fuzellier, H.; Burneau, A.; Bubessy, J.; Lelaurain, M. Sulfate Graphite Intercalation Compounds: New Electrochemical Data and Spontaneous Intercalation. *Carbon* **1995**, *33*, 123–128.
15. Shioyama, H.; Fujii, R. Electrochemical Reactions of Stage 1 Sulfuric Acid−Graphite Intercalation Compound. *Carbon* **1987**, *25*, 771–774.
16. Dimiev, A.; Bachilo, S.; Saito, R.; Tour, J. M. Reversible Formation of Ammonium Persulfate−Sulfuric Acid−Graphite Intercalation Compounds and Their Peculiar Raman Spectra. *ACS Nano* **2012**, *6*, 7842–7849.
17. Saito, R.; Jorio, A.; Souza Filho, A. G.; Dresselhaus, G.; Dresselhaus, M. S.; Pimenta, M. A. Probing Phonon Dispersion Relations of Graphite by Double Resonance Raman Scattering. *Phys. Rev. Lett.* **2002**, *88*, 027401-4.
18. Saito, R.; Grüneis, A.; Samsonidze, G. G.; Brar, V. W.; Dresselhaus, G.; Dresselhaus, M. S.; Jorio, A.; Cançado, L. G.; Fantini, C.; Pimenta, M. A.; *et al.* Double Resonance Raman Spectroscopy of Single Wall Carbon Nanotubes. *New J. Phys.* **2003**, *5*, 157.1-15.
19. Lucchese, M. M.; Stavale, F.; Martins Ferreira, E. H.; Vilani, C.; Moutinho, M. V. O.; Capaz, R. B.; Achete, C. A.; Jorio, A. Quantifying Ion-Induced Defects and Raman Relaxation Length in Graphene. *Carbon* **2010**, *48*, 1592–1597.
20. Cançado, L. G.; Jorio, A.; Martins Ferreira, E. H.; Stavale, F.; Achete, C. A.; Capaz, R. B.; Moutinho, M. V. O.; Lombardo, A.; Kulmala, T. S.; Ferrari, A. C. Quantifying Defects in Graphene *via* Raman Spectroscopy at Different Excitation Energies. *Nano Lett.* **2011**, *11*, 3190–3196.
21. Ferrari, A. C.; Robertson, J. Interpretation of Raman Spectra of Disordered and Amorphous Carbon. *Phys. Rev. B* **2011**, *61*, 14095-13.